ELSEVIER

2609

Multiscale Assessment of Binary and Continuous Landcover Variables for MODIS Validation, Mapping, and Modeling Applications

Bruce T. Milne and Warren B. Cohen†*

Validation, mapping, and modeling efforts require accurate methods to transform process rates and ecosystem attributes estimated from small field plots to the 250–1000-m-wide cells used by a new generation of land cover mapping sensors. We provide alternative scale transformations, each with attendant assumptions and limitations. The choice of method depends on spatial characteristics of the land cover variables in question and consequently may vary between biomes or with the intended application. We extend the fractal similarity dimension renormalization method, previously developed for binary maps, to continuous variables. The method can preserve both the mean and the multifractal properties of the image, thereby satisfying a major goal, namely, to provide accurate areal estimates without sacrificing information about within-site variation. The scale transformation enables the multifractal scaling exponents of landscapes or individual spectral bands to be brought in and out of register with each other, thereby opening another dimension upon which to detect the scales at which various land use or terrain processes operate. Alternatively, landscapes can be selectively rescaled to highlight patterns due to particular processes. We recommend geostatistical procedures with which to assess spatial characteristics both within a site and within individual image cells. We recommend that aggregation of fine-grain measurements during validation of the Moderate Resolution Imaging Spectrometer (MODIS) products be based on continuous variables to reduce errors that originate from uncertainties in binary maps. ©*Elsevier Science Inc., 1999*

INTRODUCTION

Accurate determination of global net carbon flux is perhaps the most urgent issue facing the ecological community (Churkina and Running, 1998). Loading the atmosphere with carbon in excess of the biosphere's steady state cycling capacity has many well-known implications, including increases in global temperature (Schlesinger, 1991). The capacity of the biosphere for carbon involves interactions among various processes such as water and energy supply, nutrient cycling, production, storage, and respiration. Remote sensing combined with process modeling and field validation offers the only currently feasible approach for assessing ecosystem capacities for carbon over vast regions. However, many crucial assumptions are made in the course of relating field measurements to the grid cells used in remote sensing (Box et al., 1989). Accuracy assessment is virtually impossible without expressions for the discrepancies between estimates obtained from field plots and from remotely sensed imagery. The problem is compounded when the grid cells are large (60–1000 m) as is the case for the next generation of sensors, such as the Moderate Resolution Imaging Spectrometer (MODIS; Ustin et al., 1991).

*Department of Biology, University of New Mexico, Albuquerque
†USDA Forest Service, Pacific Northwest Research Station, Forestry Sciences Laboratory, Corvallis, Oregon

Address correspondence to B. T. Milne, Department of Biology, University of New Mexico, Albuquerque, NM 87131. E-mail: bmilne@sevilleta.unm.edu

Received 15 May 1998; revised 30 March 1999.

REMOTE SENS. ENVIRON. 70:82–98 (1999)

655 Avenue of the Americas, New York, NY 10010

0034-4257/99/$–see front matter
PII S0034-4257(99)00059-0

Table 1. Land Cover Variables Commonly Derived from Remotely Sensed Imagery for Use in Ecological Models

Variable	*Type*	*Units*	*Applications*
Land cover	Categorical, binary	ha, %	Model stratification, land use change, habitat characterization
LAI (one-sided)	Continuous	m^2/m^2	Transpirative surface in photosynthesis models
NPP	Continuous	$g\ m^{-2}\ yr^{-1}$	Estimate of carbon fixation minus respiration
Plant cover	Continuous	%	Basis of allometric relations to predict LAI; canopy models, phenology

In large cells, fluxes of energy and water may be regulated by hydrological effects that occur at subcell scales (White and Running, 1994; Rodríguez-Iturbe and Rinaldo, 1998). Thus, functional linkages within individual cells may violate the assumption that land cover types and locations are independent, thereby necessitating a nonlinear mixing model to predict carbon flux.

Based on 36 spectral bands, MODIS will provide 42 standard data products describing atmospheric, aquatic, and terrestrial conditions (Barnes et al., 1998). Of ecological interest are estimates of land cover, biophysical properties (Table 1), and hydrological inputs such as snow, that are essential in all models of carbon, energy, and water flux from ecosystems. With global coverage every 1–2 days, MODIS will provide unprecedented data of sufficient temporal resolution to unravel effects of climatic variability, anthropogenic nutrient inputs, and land use practices on global productivity, with wide application to problems of biodiversity, ecosystem organization, and landscape function.

Traditionally, ecologists have estimated biophysical variables without much regard for location, as when net primary productivity (NPP) and leaf area index (LAI) are used in nonspatial compartment models of ecosystems. However, real-space models are needed to represent the juxtaposition of sources and sinks that affect fluxes of nutrients (Cooper et al., 1987). Similarly, canopy gap structure affects radiation inputs to the soil surface (Rich et al., 1993) and nutrient cycling rates (Parsons et al., 1994). Thus, ecologists need more complete knowledge about the ability of coarse or medium resolution imagery to represent the environment.

Field estimation techniques, and the operational definitions of variables such as LAI (Barclay, 1998, Gower et al., 1999, this issue), vary widely among studies. Variation stems from physiognomic differences between biomes and vegetation types that require different measurement techniques. MODIS will provide comparability among biomes by providing simultaneous global estimates which will need to be validated using field measurements. Field estimation of productivity and LAI is a costly, time-consuming endeavor. In the best situations estimation costs scale linearly with study size. Consequently, repeatable, accurate estimates based on remotely sensed imagery over wide regions for little cost are highly desirable, albeit subject to caveats (Baret and Guyot, 1991). Here, we demonstrate how to use high resolution Thematic Mapper (TM) imagery to prospect for large MODIS cells within which to stratify field measurements.

By alleviating the bulk of routine processing burdens (Justice et al., 1998), the 42 standard MODIS products will further increase the ecological community's use of remotely sensed estimates of biophysical quantities. Several difficult issues are entailed when coarse spatial resolution data are used. The major issue is to determine the limits to which ecological models based on spatially detailed sensors, such as TM, can be applied to coarse resolution imagery from MODIS. Adoption of MODIS amounts to a scale transformation that affects both the design of validation studies and model formulation.

Scale transformations can be viewed in two ways, either as a cartographic problem or as an ecological opportunity. First, scale transformation is problematical in that the spatial structure and corresponding geostatistical properties of a scene change with scale (Openshaw, 1984). Model calibrations developed at one scale are not readily applied at others (O'Neill and Rust, 1979; Cale et al., 1983; King et al., 1991) and may be further complicated if many variables are of interest (Pierce and Running, 1995). Errors introduced by scale transformation potentially confound estimates of net primary production (NPP), leaf area index (LAI), and land cover type which are the products from MODIS and similar sensors. Validation of coarse resolution maps with field measurements is not simple and generally lacks reliable theory to guide the process. Second, changes in apparent landscape structure with changes in scale may provide new information about the scale domains (Burrough, 1983; O'Neill et al., 1991; Milne, 1988; Johnson et al., 1992) over which particular processes operate (Jelinski and Wu, 1995). Thus, purposeful changes in scale can be used as tools to further ecological understanding of process.

This study has two general goals: 1) to identify issues concerning spatial aggregation, validation, and error assessment that will be encountered as MODIS is applied across diverse biomes, and 2) to recommend spatial aggregation methods for use in modeling and validation exercises across a wide array of sites. A major antagonism exists between the goals of projects conducted at disparate scales. Namely, the MODIS estimates of NPP, LAI, and land cover do not characterize subcell patterning that is both of interest to investigators at particular sites

and a potential source of error at the 500–1000 m scale. Thus, a focus of this article is to assess patterns within cells that may alter MODIS estimates and simultaneously limit the utility of MODIS estimates of biophysical properties at finer scales.

STATISTICAL AND PROCESS ORIENTED APPROACHES

Over several decades, two major bodies of theory have developed in parallel to explain and exploit spatial variability for many purposes. The first, geostatistics (Cressie, 1991; Deutsch and Journel, 1992), has wide application in the earth sciences, ecology, and the mining industry. Geostatistics characterize spatial distributions of one or more variables, so that point measurements can be extrapolated to unmeasured locations, as when prospecting. Generally, the geostatistical extrapolations rely on systems of equations or stochastic processes (Deutsch and Journel, 1992) to obtain unbiased estimates of ore densities, biomass, or other variables from scattered point measurements. Fractal geometry (Mandelbrot, 1982) is the second major theory of spatial structure and organization that is applied readily to terrain, river networks (Rodríguez-Iturbe and Rinaldo, 1998) coastlines, clouds, and myriad other systems (Feder, 1988). Although fractal geometry is used simply to describe patterns at many scales, several studies have focused on the intimate links between dynamics and structure, to the point of demonstrating how energy dissipation produces fractal structures (e.g., Jensen et al., 1985; Sommerer and Ott, 1993; Rodríguez-Iturbe and Rinaldo, 1998). Recent derivations of fractal scaling laws via the renormalization group (Wilson, 1979; Binney et al., 1993) rely on detailed descriptions of stochastic processes and purposeful changes in scale (Loreto et al., 1995). Despite several superficial links between geostatistics and fractals (e.g., Burrough, 1981), there is little theory to link the two fields. Given that virtually all fractal and renormalization approaches entail many to one mappings, or regularizations, it is reasonable to expect a synthesis of regularization theory with fractals and the renormalization group so that both the statistical depth and process based explanations of spatial complexity can be applied simultaneously. As a first attempt, this article treads in both arenas, primarily by applying fractal geometry and renormalization theory to derive an expression for the geostatistics of indicator maps, which are at the root of regularization theory.

Regularization theory (Jupp et al., 1988a,b) provides a single theoretical basis for the geostatistical properties of both remotely sensed imagery and the selection of field samples that are used to validate imagery. Formally, we envision a random field $f(\mathbf{x})$, where $\mathbf{x}$ is a vector in space, time, or both, and $f(\mathbf{x})$ is a realization of an ergodic, spatially continuous stochastic process with stationary parameters. Then, both remote sensing and field sampling amount to regularizations (*sensu* Jupp et al., 1988a,b; Atkinson and Curran, 1995), by which spatially integrated or averaged measures of the random field are represented on a discrete lattice, that is, $f(\mathbf{x})$ at many points within each lattice cell (or image pixel) of length L are mapped into a single value. Thus, the radiant field is convolved with the sampling function of the sensor to produce an image $g(f(\mathbf{x}),L)$. Clearly, spatial autocorrelation affects the distribution of $f(\mathbf{x})$ within the cell and therefore the mean value in the cell. Regularization theory is concerned with the statistical behavior of spatial autocorrelation and semivariance as functions of cell length, or scale. The theory can: 1) be used to identify cell lengths that best enable detection of pattern (e.g., Hill, 1973), 2) characterize how variance changes with scale, as needed for geostatistical interpolation, and 3) design field sampling strategies that minimize the number of subsamples needed to estimate mean quantities such as biomass or leaf area index.

SPATIAL VARIABILITY

In an ideal world, land cover, NPP, LAI, and percent live plant cover would be homogeneously distributed across the Earth's surface so that mean values and variances could be measured with quadrats of any size. Of course, geological and biophysical quantities are generally correlated through space and time, giving rise to nonrandom structure, patches, and clines. Spatial correlations necessitate the use of geostatistics to extrapolate measurements (Cressie, 1991; Deutsch and Journel, 1992). Spatial and temporal (Bilonick, 1985) variation are characterized by the semivariance $\gamma(h)$, which is the mean squared deviation of a variable at locations separated by a given lag distance:

$$\gamma(h)=1/(2N(h)) \sum_{i=1}^{N(h)} (z_i-z_{i+h})^{\lambda}, \qquad (1)$$

where z_i is the variable at location i, $N(h)$ is the number of pairs of points separated by distance h and λ is an exponent equal to 2 for the classical semivariance. A semivariogram is a graph of the semivariance versus lag. Setting λ equal to 1/2 produces the semirodogram, while $\lambda=1$ applied to the absolute value $|z_i-z_{i+h}|$ produces the semimadogram. These variograms emphasize broad scale structure, such as the lag at which the semivariance reaches an asymptote (i.e., the range; Cressie, 1991; Deutsch and Journel, 1992). The indicator semivariance is measured by transforming z_i to 1 if $z_i \geq$ a threshold and 0 otherwise. Thus, the indicator semivariance is essentially that of a binary map, and thereby characterizes patterns of nominal variables.

The semivariance is relatively small when a variable is correlated through space. Sampling with quadrats as wide as the range ensures that autocorrelation is sub-

sumed, leaving statistically homogeneous sampling units that meet the assumption of independence (Hurlbert, 1984). In general, though, ecological studies that focus on causal factors seek predictable relations between system properties measured in small quadrats in the field (e.g., soil moisture and stomatal conductance). Unfortunately, the homogeneity condition means that the variation within quadrats is as large as that among quadrats, leading to nonsignificant models of system properties based on remotely sensed measurements for which the cell size may exceed the semivariogram range of field measurements (Friedl et al., 1995). Moreover, an assumption of a finite variance cannot be made where the semivariance fails to reach an asymptote, as for example along clines or within fractals (Mandelbrot, 1982). Comparisons [Eq. (1)] along north–south versus east–west orientations may produce different semivariograms due to anisotropy, further complicating the statistical characterization of pattern.

Parametric interpolations based on the relation between semivariance and lag may entail an assumption of stationarity, or constant statistical conditions throughout the study area. Deutsch and Journel (1992) argue that stationarity is an assumption implicit in parametric models, while nature may exhibit patterns for which parametric models are not readily constructed. Here, stationarity, or the lack thereof, may affect various aggregation strategies and perhaps the accuracy of the MODIS sensor, in that behavior of a given method or sensor may vary throughout a map, or within pixels, generally in unknown ways (e.g., Stoms et al., 1997).

A major insight from regularization theory is that the length of a lattice cell, or pixel, affects precision directly according to

$$\gamma(h,L) \simeq \gamma(h) - \bar{\gamma}(L^2),$$

where $\gamma(h,L)$ is the semivariance at lag h measured using (image) cells of length L, $\gamma(h)$ is the parametric semivariance of the spatially continuous field $f(\mathbf{x})$, and $\bar{\gamma}(L^2)$ is the within-cell mean semivariance; L^2 indicates that averaging is over the area of the cell (Atkinson and Curran, 1995). Thus, regularization to cells of finite area decreases the image semivariance in proportion to L^{-2} (Jupp et al., 1988a).

A second conclusion is that regularization entails a many to one mapping of $f(\mathbf{x})$ into $g(f(\mathbf{x}),L)$ and thus a reduction in the variance from which to mine predictive relations between variables. For example, if we wish to predict LAI at a sample point, we might begin with an image measure of the normalized difference vegetation index (NDVI) and the relation LAI=f(NDVI). Of course, regularization has mapped a region L^2 of NDVI values to a single NDVI′, and an error will occur of size LAI$-f$(NDVI′). Recent applications of renormalization to terrain (Rodríguez-Iturbe and Rinaldo, 1998) show that judicial rescaling of drainage networks can preserve statistical properties of the map, while arbitrary regularizations of the elevation field do not. Thus, empirical and theoretical studies of regularization should identify useful scale transformations that preserve information needed to model landscape processes accurately. The exact regularization procedure will depend on the purpose.

Considering the accuracy of MODIS measurements, some major issues are: 1) whether MODIS estimates of land cover variables (Table 1) are affected by within cell structure, 2) how to avoid biased MODIS estimates that may occur within a scene, and 3) how to use *a priori* assessments of spatial variation to minimize field sampling efforts related to MODIS validation. We address these issues primarily through empirical studies of imagery and simulated regularizations.

ANALYSES

Our discussion of spatial analysis focuses on characterizations of within-cell variation to reduce the number of field sampling locations needed for estimates of mean values over a study area. We also consider components of the semivariogram, such as the nugget, which can be decomposed to represent processes that contribute to pattern at various scales.

Within-Cell Variation

We examined within-cell structure via semivariance analysis of the Sevilleta LAI map and maps of the normalized difference vegetation index (NDVI) for the Konza Prairie and H. J. Andrews Long Term Ecological Research sites (LTER; Franklin et al., 1990). The three LTER sites represent a broad gradient ranging from semiarid grasslands (Sevilleta), to tallgrass prairie (Konza), to conifer forest (Andrews), and thus provide a wide range of vegetated conditions, both in absolute quantity of biomass and spatial structure. We used 100 km^2 subregions of the LTER sites for intensive studies.

The Sevilleta LAI map was created from an unsupervised classification of 12 NDVI images, stratified by season, from TM imagery. Field samples in support of the mapping effort were obtained from 22 m diameter plots stratified randomly among 30 classes. Percent cover and height of each species, classified into guilds (i.e., forb, C_3 grass, C_4 grass, shrub, and *Larrea tridentata*, a major shrub species which was treated separately) were used in regressions to calculate LAI (P. Kemp, personal communication). Each spectral class was then described by the mean LAI obtained from replicate field samples of that class. Thus, the Sevilleta LAI map shows the mean LAI of the respective class.

To assess geostatistical variability within a biome, we created one semivariogram for the Sevilleta LAI map using lags $\leq$3.3 km (Figs. 1a and 2a). We hypothesized that one or more break points would be found separating

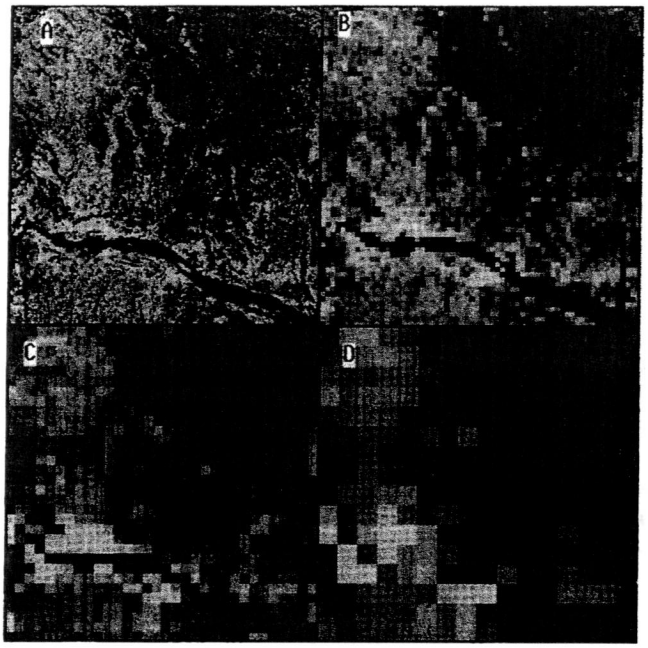

Figure 1. Leaf area index for a 5325 ha portion of the Sevilleta Long Term Ecological Research site. Brightness is proportional to LAI. A) Original 28.5 m resolution; B) second renormalized image [see Eq. (6)] to 114 m cell width; C) continued renormalizations to 228 m; D) 456 m resolution.

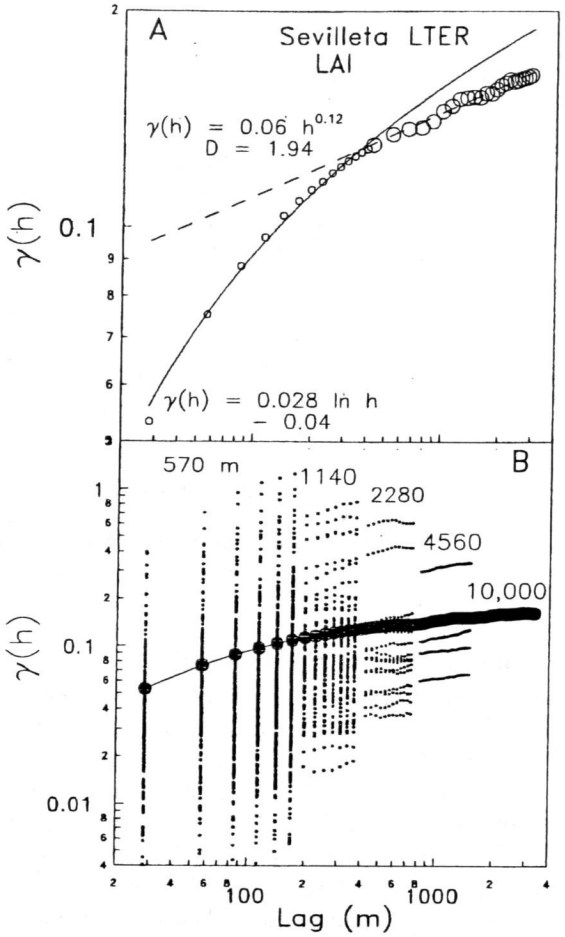

Figure 2. Semivariance of leaf area index (LAI) in the Sevilleta LTER. A) Analysis of 28.4 m wide cells obtained from Landsat Thematic Mapper imagery; B) variation among semivariograms of LAI in the 28.4 m wide cells within the entire 10,000 m^2 area (large dots) and within successively larger pseudo-MODIS cells ranging from 570 m to 10,000 m in length.

scale domains (O'Neill et al., 1991) over which different semivariogram models would need to be fit to minimize the sum of squared residuals. We followed Stauffer and Stanley (1989) and identified a critical lag in the semivariogram by examining residuals from logarithmic and power laws that were fit preliminarily over the entire domain of lags. The critical lag was readily identified by residuals equal to zero; increasing residuals away from the critical lag indicated systematic errors that were readily corrected by fitting different models below and above the critical lag. With two models, the sum of squared residuals over both domains was less than that obtained from any single model.

The semivariance did not reach an asymptote at lags <400 m (Fig. 2a), and was well characterized by a logarithmic model. Thus, we expect field measurements to be correlated if separated by distances less than the MODIS cell size. At lags >400 m, a power law fit the semivariances well (Fig. 2a), suggesting that LAI at the Sevilleta exhibits fractal properties at these scales (Mandelbrot, 1982, Burrough, 1981, Milne, 1991). Apparently, fractal terrain with associated variation in soil resources, controls plant patterning at broad scales. Since the semivariance did not reach an asymptote, no TM cells can be considered independent. By the same token, the strong autocorrelation at lags <400 m indicated less variation within MODIS pixels than among them. Thus, we hypothesized that relatively few subsamples would be needed within a MODIS cell to characterize LAI for validation purposes.

We evaluated this hypothesis by pooling TM cells to form pseudo-MODIS cells (hereafter pMODIS cells) of various widths. We then examined variation among semivariograms obtained within pMODIS cells (Fig. 2b). For any given lag, semivariances varied over 2 orders of magnitude. High semivariances within pMODIS cells occurred where several contrasting land cover types converged, as where dry streambeds, riparian woodlands, and grasslands intersected (Fig. 1a). Repeated semivariance analysis within larger and larger pMODIS cells revealed a convergence of within-cell semivariograms on the semivariogram for the entire study area, such that the semivariograms from the four pMODIS cells of length 4560 m were more similar to the overall semivariogram than were those from the smaller pMODIS cells. Thus, variation among high resolution cells should be greater than among low resolution cells (Levin, 1992).

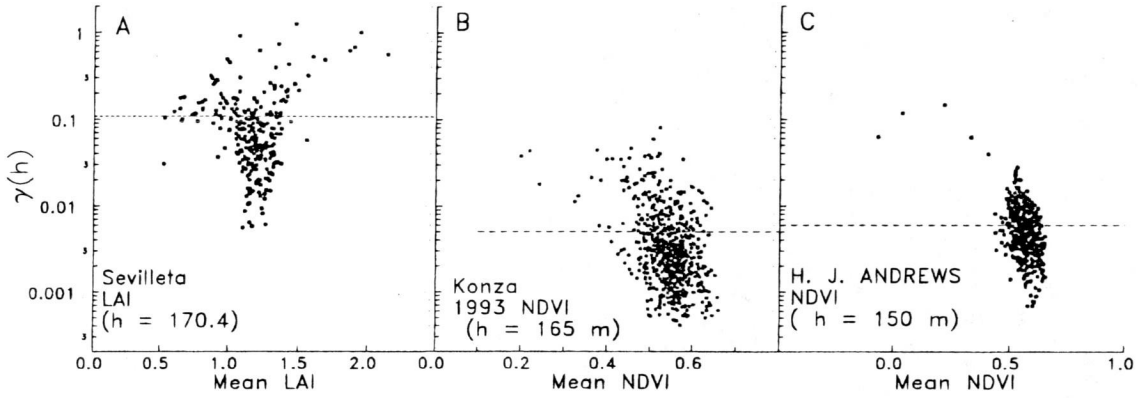

Figure 3. Semivariances at selected lag distances and mean values of leaf area index and NDVI from the Sevilleta, Konza Prairie, and H. J. Andrews LTER sites. Semivariances and means were computed from TM cells within 500 m wide pseudo MODIS cells. The dashed line indicates the semivariance of TM cells over the entire image at the specified lag, h.

Sample Points for Field Samples

Validation efforts require sample points that efficiently estimate statistical properties such as mean biomass or LAI for comparison with MODIS estimates. One strategy is to target MODIS cells that are internally homogeneous, thereby requiring fewer samples to characterize the cell. To determine how within-cell variation affects estimates of the mean, we used TM maps of LAI (Sevilleta) and NDVI (Konza and Andrews) to measure and compare the semivariance and mean within pMODIS cells. Data management practices that include resampling of imagery to match other archived data, such as terrain and soil maps at the Sevilleta, Konza, and Andrews sites, provided TM cell sizes of 28.4 m, 33.0 m, and 25.0 m, respectively (Fig. 3). Since we were interested in the highest semivariance that could be encountered within a pMODIS cell, but wanted to avoid artifacts from using too large a lag, we honored Nyquist sampling theory and restricted our lag to ~500/3 m (O'Neill et al., 1996), thereby using 170.4 m, 165 m, and 150 m lags for the Sevilleta, Konza, and Andrews, respectively. For reference, we used the corresponding semivariance from an analysis of all the TM cells within each 100 km^2 study area. Preferred pMODIS cells for validation efforts were those with less variability than the reference.

In the Sevilleta, cells with $\gamma(170.4)$ below 0.108 were remarkably close to the mean LAI (Fig. 3a). Cells with low semivariance have uniform canopies, of either grass or mixtures of shrubs and grass. Greater scatter and a significant correlation between semivariance and mean LAI was apparent for $\gamma(170.4)>0.108$ ($r=0.49$, $n=84$, $P=0.002$). These highly variable pMODIS cells contain mixtures of saltcedar (*Tamarix pentandra*) stands along seasonally dry riverbeds adjacent to low LAI grasslands (30–40% cover) and sparse shrublands.

Thus, field efforts to assess MODIS accuracy could be minimized by stratifying samples according to within-cell variance (Fig. 3). Effort to estimate the mean LAI could be reduced by sampling from the set of MODIS cells that have small internal semivariances (e.g., $\gamma(h) \leq 0.05$). However, since sensors should perform best in such circumstances, efforts to validate the sensor should also be devoted to cells with high internal semivariances. There, nonadditive spectral effects of mixed canopies could produce biased estimates of land cover properties. We suggest that subsampling selected MODIS cells and using high resolution TM imagery to make area-adjusted estimates for the entire cell is an appropriate way of testing the accuracy of MODIS estimates. Thus, assessment of within-cell variation relative to the known LAI (Fig. 3) can guide experiments to evaluate MODIS for potential bias due to subpixel variation.

Three orders of magnitude variation in semivariance were also found for NDVI within pMODIS cells in the Konza and Andrews sites (Figs. 3b, c). These sites have many sources of variation in vegetation and biophysical traits due to successional age of the plant communities, experimental burning treatments, and terrain. Nonetheless, NDVI saturates 5–10 years after clearcut and is not meaningful with respect to LAI at Andrews or Konza (Turner et al., 1999, this issue). Even greater spatial variation would be expected for spectral variables other than NDVI, such as wetness, a component of the TM tasseled cap relation (Crist and Cicone, 1984), since wetness is highly correlated with forest structure.

Semivariogram Decomposition

The nugget variance, or the semivariance at a lag of zero, is a second useful characteristic of the semivariogram. The nugget measures the within-cell variance, sometimes interpreted as sampling error (Atkinson, 1997). Cressie (1991, pp. 112, 130) decomposes the nugget into measurement error plus variation due to stationary processes

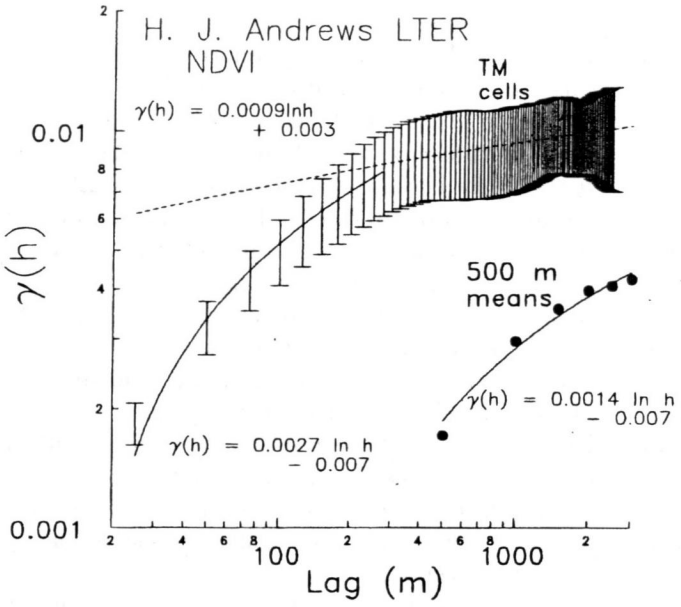

Figure 4. Semivariance of normalized difference vegetation index for the H. J. Andrews LTER based on Thematic Mapper (TM) imagery and on means of TM cells within 500 m wide blocks.

that occur at subpixel scales. For example, broad scale, among MODIS cell variation may be controlled by terrain, but variation within MODIS cells could be due to animal burrowing or treefall gaps that create microscale pattern. The subcell process has its own inherent variation at all lags shorter than the length of the cell. Here, the semivariance of TM cells characterizes the processes within the pMODIS cells. If, for example, we average NDVI from the TM cells within each pMODIS cell, then the semivariance of the mean values can be decomposed as in Eq. (2):

$$2\gamma_{\text{pMODIS}}(0)=2\gamma_{\text{TM}}(0)+2\sigma^2_{\text{error}}, \quad (2)$$

where $\gamma_{\text{TM}}(0)$ is the nugget variation of TM measurements within pMODIS cells and σ^2_{error} is the variance of the measurement error associated with TM cells.

Similarly, the decomposition can be applied to the entire semivariogram, in which case [Eq. (3)]

$$2\gamma_{\text{pMODIS}}(h)=2\gamma_{W}(h)+2\gamma_{\text{TM}}(h)+2\sigma^2_{\text{error}}, \quad (3)$$

which includes variation due to a smoothly varying process (W) whose semivariogram range is greater than the distance between adjacent pMODIS cells; that is, it contributes to autocorrelation among the pMODIS cells. This decomposition provides an hypothesis for evaluating transformations of maps from fine to coarse resolution; namely, the semivariance of the coarse resolution image should be related to the variance of finer grained measurements taken within the cells.

As an example, we used NDVI measurements of the Andrews and evaluated the relationship between the semivariogram of the TM cells and the semivariogram of mean NDVI calculated within 500-m-wide pMODIS cells. Based on smaller TM cells, the within-pMODIS semivariance was greater than that among means extracted from pMODIS cells (Fig. 4). An explanation for this comes from the related observation that two logarithmic models were needed to characterize the semivariogram of TM cells (Fig. 4). The logarithmic model that fit semivariances for lags <400 m shared similar coefficients to that of the semivariogram for means from pMODIS cells (Fig. 4). Thus, averaging NDVI within pMODIS cells cast the geostatistical properties of the fine scale TM imagery up to the pMODIS cells. If the MODIS sensor effectively averages, then we predict that geostatistical properties of MODIS images will be fit by the same semivariogram formulae used for high resolution images analyzed with lags ≤the length of MODIS cells (see also Jupp et al., 1988b). Thus, if averaging occurs, MODIS should capture fine scale geostatistical properties of surface roughness and ground cover while rendering them at relatively coarse scales. In other terms, averaging may protect variation among the large cells from attaining the range, and thereby preserve the ability of independent variables to predict ecological responses, such as NPP, at the broad scale.

In summary, the semivariance analyses illustrate the magnitude and nature of variation that can be expected within MODIS cells. Sampling efforts can be minimized where semivariances are small and can be exploited to test MODIS estimates where they are large. The simplest null hypothesis is that the accuracy of MODIS estimates is the same regardless of within-cell variation. Evaluations across sites might reveal interactions between biome and semivariance, possibly due to saturation of NDVI at high LAI values in forested regions. Given these considerations, we next review various spatial aggregation methods by which fine scale data can be cast to cell sizes comparable to MODIS products, gener-

ally for use in models to predict NPP for comparison with MODIS.

AGGREGATION METHODS

There are many challenges in the transformation of ecosystem characteristics from fine to coarse scales. One challenge stems from the idiosyncracies of the land cover variables themselves (Table 1). Units of measure differ among the variables, so care must be taken to construct rescaling procedures that preserve the units of measure so that the resulting map remains useful for modeling. Here, we divide the variables into two categories: binary and continuous. For example, a typical thematic vegetation map is the union of a set of binary maps; pixels are coded as one and only one vegetation type. In practice, the many binary maps implicit in a thematic map can be translated into multivariate continuous measures by moving window techniques (Milne, 1991) or logistic regression (Strauss, 1992). In contrast, continuous variables such as elevation, LAI, and potential evapotranspiration require aggregation techniques that preserve the units of measure and statistical moments such as the mean. Here, we address the various aggregation alternatives in turn and use spatial renormalization theory to derive an approximation of the semivariance of random maps and thereby link the renormalization aggregation methodology with classical geostatistics.

Binary Variables

The simplest land cover map is binary, in which cells have one of two states. A thematic map is simply the union of several binary maps. Various intuitively reasonable aggregation approaches can be used (e.g., nearest neighbor resampling, majority rule, presence/absence; Turner, 1989) in concert with theoretical frameworks to manipulate the aggregation process (Milne et al., 1999). Here we present a proportional reclassification method and review spatial renormalization of binary maps in anticipation of a continuous renormalization method to follow.

Proportional reclassification to a coarser scale begins with a thematic map obtained at relatively fine scale (Fig. 5). Then, a coarse grid is superimposed on the map and the proportion of each class within each coarse cell is determined. Thus, several new maps describe the relative proportions of each class. The resulting vectors of proportions can be subjected to cluster analysis to obtain a cover map at the coarse scale or can be used as dependent variables in regression models to investigate the effects of independent variables on landscape composition.

Aggregation strategies benefit from the broader theory of renormalization (Gould and Tobochnik, 1988; Creswick et al., 1992; Binney et al., 1993; Milne and Johnson, 1993; Milne, 1998). Renormalization was developed in studies of critical phenomena in physics, where phase transitions occur at particular densities or temperatures. In these situations, models based on averages cannot characterize the geometric properties of the system, largely because spatial correlations exist over vast distances and there is no particular scale or quadrat size in which to estimate a mean or variance. A homologous problem occurs when assumptions of geostatistical stationarity are not valid or when variance increases steadily with scale (Mandelbrot and Wallis, 1969); both are common in nature and notoriously difficult to represent by Gausian distributions (e.g., Stanley et al., 1996). Because landscapes share phase transition properties with physical systems (Milne et al., 1996; Keitt et al., 1997), the theoretical depth of renormalization provides tools for solving many scale transformation problems in ecology and remote sensing.

A successful renormalization involves identification of a quintessential property of a system to preserve while reducing the number of cells on a map. After renormalization, the map will retain a particular property if it was there to begin with. In that sense, renormalization can be viewed as a multiscale filter. For example, the nitrogen fixing capabilities of *Alnus* make it a biologically significant component of the Pacific Northwest landscape. Since alder covers <5% of the landscape, some aggregation procedures, such as the majority rule, would eliminate the smallest alder patches in translations of 25 m cells to 1 km (Benson and MacKenzie, 1995). However, use of a presence/absence rule would ensure its occurrence on the coarse map.

The rate at which information is degraded by renormalization can be assessed. There are two cases: 1) when the states of cells are independent and 2) when autocorrelation exists among the cells. When cells are independent, simple analytical expressions can be written for the changes in land cover with changes in cell length, that is, when the nugget of the indicator semivariance equals the variance or when cell width exceeds the range. For example, consider the majority rule implemented by dividing a binary map into blocks of 2 by 2 cells. Occupied cells occur in various configurations, including the four ways of having one occupied cell, six ways of having two occupied cells, four ways of having three occupied cells, and one way of having all four occupied (Gould and Tobochnik, 1988). Any block of cells that has a majority of occupied cells is reclassified as occupied. Of course, since occupied cells occur with probability p and unoccupied cells with probability $1-p$, a particular configuration, say three occupied and one unoccupied cell, occurs with probability $4p^3(1-p)$. Thus, assuming independence, we can write a renormalization function to describe the proportion of occupied blocks after one application of the rule:

$$p' = \tfrac{1}{2}6p^2(1-p)^2 + 4p^3(1-p) + p^4$$

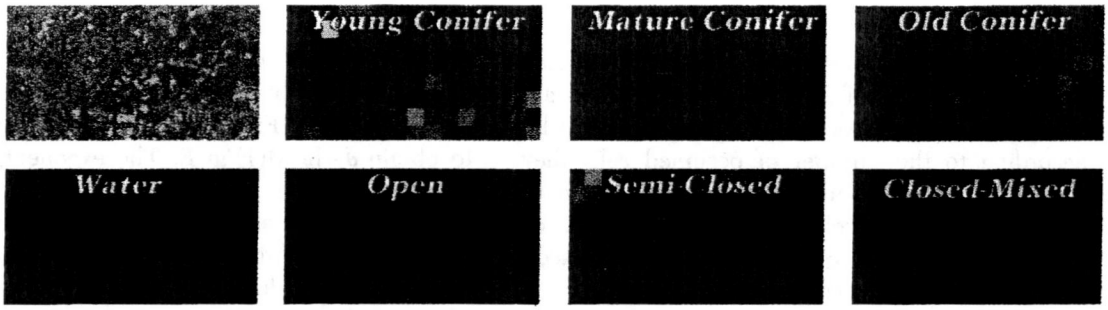

Figure 5. Proportional reclassification of the H. J. Andrews MODLERS site cover map. The original map (upper left) was developed from Landsat TM data and has a cell size of 25 m (Cohen et al., 1995). Tallies of each class within nonoverlapping 1-km-wide cells were mapped separately in hues that correspond to the TM classification color scheme. Intensity of the derived maps is proportional to the relative proportion of the class in the cell.

$$=3p^2(1-p)^2+4p^3(1-p)+p^4$$
$$=p^2(3-2p), \quad (4)$$

where the coefficient in the first term accommodates ties when two cells are occupied. Thus, we can write other renormalization rules (Milne and Johnson, 1993) and apply them for scale transformation when cells are independent. Unfortunately, independence is a special case, and does not exist at lags shorter than the range (Fig. 2). Thus, other characterizations must be made for empirical systems.

The so-called box scaling relation (Feder, 1988) is an effective and simple aggregation expression for fractal landscapes in which autocorrelation exists and a simple presence/absence aggregation rule suffices. For example, models of stream biogeochemistry and validation of MODIS imagery would seem to require maps of nitrogen fixing trees at very fine scale. Thus, a presence/absence renormalization could be applied by inspecting each 2 by 2 block of cells on a map and retaining the entire block if it contains at least one cell occupied by alder. Since stream geometry and flow induce both statistical and functional autocorrelation, respectively, the simple probabilistic representation [Eq. (4)] of scale dependence cannot be used. Rather, we tally the number of blocks occupied as the map is subjected to a series of renormalizations. Cells are first aggregated into blocks of 2 by 2 cells, and then blocks of 2 by 2 blocks are aggregated, to represent 16 cells, etc. For fractal patterns, the number of occupied blocks $N(L)$ of length L scales as kL^{-D}, where k is a constant and D is the box fractal dimension. The number of blocks (i.e., boxes in the fractal literature) can be expressed as a probability by dividing $N(L)$ by $(E/L)^2$, which is the number of boxes that could fit on a square map of length, or extent, E. Substitution from the scaling relation gives

$$p'(L)=(k/E^2)L^{2-D}. \quad (5)$$

Thus, both a statistical characterization and maps at each scale are produced for modeling purposes.

Although the binary representation of the landscape may not be very useful when rendered so coarsely, occupied blocks for large L indicate where a more complete or detailed representation of relevant processes is warranted. Multiscale approaches are very useful in ecology, in which a complete system model may be composed of submodels in different forms (e.g., ordinary differential equations, individual based models) rendered at spatial and temporal scales that may vary among submodels. For example, where physical conditions change abruptly, as at ecotones, higher spatial resolution may be required to accommodate large within-cell variance (Milne et al., 1996). Large semivariances within a block (Fig. 2b) may indicate the presence of some large structure, such as a river, that traverses the block. Such structures are ecologically important because they regulate flows of matter and energy across landscapes (Forman, 1995). In modeling effects of water and energy supply on ecosystem processes, it is desirable to represent the structures created by several cells together, as, for example, on terrain maps, where distant peaks affect energy inputs via shading (Dubayah, 1994). Thus, the probability scaling relation [Eq. (5)] for binary maps provides information analogous to the semivariance [Eq. (1)] for continuous measures.

In anticipation of a new aggregation technique for continuous variables, described below, we briefly review Milne and Johnson's (1993) renormalization technique that maintains the similarity fractal dimension, and thus among-cell correlations, as a binary map is aggregated. For $L=1$ we define the similarity dimension $D(1)=\ln N/\ln E$ (Mandelbrot, 1982), which is the ratio of the logarithmic number of occupied cells to the logarithmic extent of the map. At coarser resolution, we expect the proportion of the occupied map to vary as in Eq. (5). Thus the number of occupied cells needed to satisfy the scaling relation is $R(L)=(E/L)^{D(1)}$ for $L\geq 2$. The goal is to place $R(L)$ occupied cells on the coarser resolution map in such a way as to preserve as much as possible the spatial autocorrelation of the finer resolution map.

In practice, the renormalization begins by identifying all nonoverlapping blocks of 2×2 cells (where blocks are now of length L and cells of length $L/2$); blocks are labeled according to the number of occupied cells they contain. Then, a frequency distribution is generated to describe the number of blocks $f(m)$ with $m=4$, 3, 2, or 1 occupied cells. Next, $f(4)$ of the $R(L)$ cells are placed in the blocks of length L that have four occupied cells. Once those are satisfied, the $R(L)-f(4)$ remaining cells are allocated to the blocks with the highest occupancy rates until a frequency class that cannot be completely allocated is found. Then, the remainder of $R(L)$ cells are allocated randomly to blocks of the incomplete class. The end result is a renormalized map that preserves the broad scale correlations and minimizes the rate of change $dp'(L)/dL$ (Milne and Johnson, 1993), thereby reducing distortion of the map. Such aggregations are of use when a model at coarse scale is expressed in terms of parameters that are highly variable at fine scales.

Continuous Variables

Models of net primary production are driven by continuous variables that capture relevant aspects of vegetation structure or energy supply (Prince and Goward, 1995) at arbitrarily coarse resolution. For example, surface roughness and shade are structural features that affect water flux and the energy balance within the canopy (Jensen et al., 1989), yet such variation is easily subsumed at 30−1000 m cell sizes. Here, we present a spatial aggregation method that preserves geometrical aspects of land cover so that the relevant consequences of aerodynamics and radiation fluxes can be represented meaningfully in models. Fortunately, canopies exhibit statistically regular, predictable changes in geometry with scale (Milne, 1991; Milne et al., 1996; Menenti et al., 1996; Pachepsky et al., 1997) that we exploited in a new aggregation method suitable for continuous measures such as LAI.

Our method preserves both the mean and the spatial arrangement of a continuous variable over the study area. We use a scaling exponent, namely, the Lipschitz–Hölder exponent (Mandelbrot, 1982; Feder, 1988) to characterize the relationship between scale, or cell length L, and the local concentration of the variable. By preserving the mean at each scale, the method avoids bias that might otherwise creep into a coarse resolution map, as, for example, by local averaging.

At successively coarser scales, we obtain new values of a continuous variable z_i in each cell $i=1, 2, 3, \ldots, n(L)$ by aggregating cells in a $\log_2$ series, for example, $L=2, 4, 8, \ldots$. Following the logic of Milne and Johnson's (1993) preservation of a scaling exponent across many cell sizes, we conserve the sum, or "mass," $M(1)=\Sigma\ z_i$ of a continuous variable over the landscape by allocating a renormalized mass $M(L)=(E/L)^{\delta}$ among the new, larger cells, where E is the number of unit cells along one edge of a square map and δ is obtained at the unit scale $L=1$. First we sum the continuous variable z_i to obtain $\delta=\ln M(1)/\ln E$. The exponent δ is then used to constrain the allocation of the renormalized mass $M(L)$ for $L\geq 2$ to each of the new, larger cells throughout the aggregation process. Thus, the portion of the integral in each cell of length L is $p_i(L)=\Sigma\ z_j(L/2)/\Sigma\ z_i(L/2)$, where 1) the numerator is summed over all four cells of length $L/2$ that compose the new block of length L, 2) the denominator is summed over all cells on the map such that $\Sigma p_i(L)=1$. A second exponent, the Lipschitz–Hölder exponent, is used to express $p_i(L)$ as a function of L, that is, $p_i=L^{a}$ (Mandelbrot, 1982), where a has an implicit subscript i. Thus, new cells of length L are assigned a renormalized value $z_i(L)$ by prorating a portion of the renormalized sum to each:

$$\begin{aligned} z_i(L) &= p_i(L)M(L) \\ &= L^{a-\delta}E^{\delta} \end{aligned} \qquad (6)$$

Allocation of $M(L)$ to each cell is both a function of the local density, which preserves the spatial pattern over the image, and the global mass, represented by E^{δ}.

As an example, a square 5323 ha region ($E=256$) of the Sevilleta LAI map was rescaled to coarse resolution following Eq. (6) (Fig. 1). After rescaling to 456 m resolution, the mean LAI equaled 93% of the mean LAI (1.147) at 28.5 m. A t-test for differences between mean LAI at the two scales, assuming unequal variances, gave $t=0.143$ ($p>0.05$), indicating that the original mean was preserved.

Given its reliance on a, the renormalization should preserve not only the mean value but also the geometrical properties of the image. We used multifractal measures (Halsey et al., 1986; Feder, 1988) to characterize the geometry and to study its behavior with changes in scale. Multifractals enable an image to be partitioned into subsets of varying intensity, thereby enabling the fractal geometry of each subset to be described independently. Partitioning leads to the notion of an image as the union of a set of images that are nonzero in some locations and zero in most others. The partitions are indexed by q with which the set of associated cells that contain nonzero values number $N(q,\varepsilon)$, where ε is the fraction of the extent occupied by a single cell. By definition, the mass exponent

$$\tau(q) = -\lim_{\varepsilon\to 0}\frac{\ln N(q,\varepsilon)}{\ln \varepsilon} = -\lim_{(E/L)^{-1}\to 0}\frac{\ln \sum p_i^{q}(L)}{\ln (E/L)^{-1}} \qquad (7)$$

characterizes the scaling behavior of many subsets of the image, indexed by q. Low values of q emphasize small $p_i(L)$ and high q emphasize large values. When $q=0$, the summands in Eq. (7) all equal 1, thereby providing a count of nonzero cells. When all $z_i(L)>0$, $\tau(q)=2$, which is the dimension of the plane in which the image resides. In the limit as $L\to 0$, the exponent forms a monotonic,

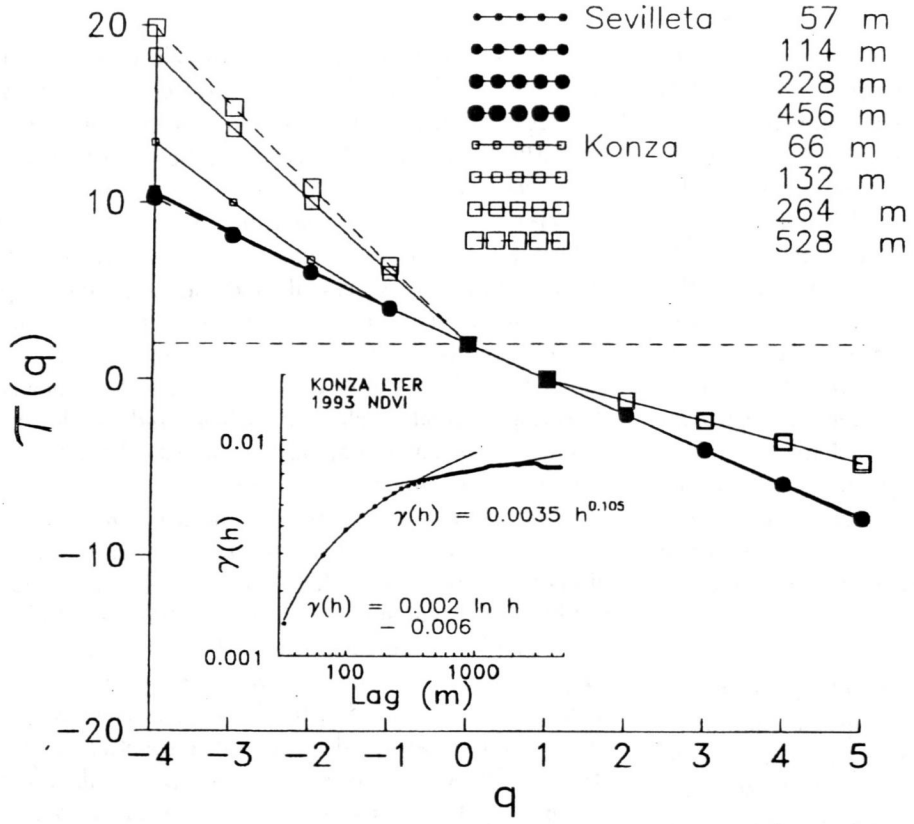

Figure 6. Mass exponents $\tau(q)$ for maps of leaf area index and normalized difference vegetation index (NDVI) from the Sevilleta and Konza LTERs, respectively. Each curve represents exponents obtained after renormalization of images to larger cell widths. Inset: semivariogram of NDVI for the Konza LTER.

decreasing function of q (Halsey et al., 1986). Thus, deviations between the $\tau(q)$ curves obtained at various L provide measures of aggregation error.

Under renormalization, the Sevilleta LAI map exhibited a remarkable preservation of the $\tau(q)$ function (Fig. 6), indicating that the coarse resolution map contained the same geometrical structure, or more specifically, partitioning of LAI among cells, as the finest scale map. Given the reiterative fashion in which the renormalized mass is constructed [Eq. (6)], and the consequent lumping of adjacent cells over hundreds of meters, the constant spectrum of mass exponents indicates that much of the geometry present at the finest scale in the Sevilleta has been preserved. Such is not always the case. In applying the renormalization to the Konza NDVI image (Fig. 7), we found changes in $\tau(q)$ with L (Fig. 6). First, the finest scale Konza map had a different $\tau(q)$ curve from that of the Sevilleta LAI for $q<0$, suggesting that low NDVI values at Konza and low LAI at Sevilleta were governed by different processes at that scale (see Solé and Manrubia, 1995); curves were indistinguishable for $q>0$. For negative q the visually apparent differences in the distributions of low LAI and NDVI values on the two landscapes (Figs. 1a and 7a) explain differences in the mass exponents (Fig. 6). Interestingly, renormalization to $L=132$ m (Fig. 7b) brought the Konza $\tau(q)$ curve precisely onto that of the Sevilleta for all q, while further renormalization moved the Konza curve off the Sevilleta

Figure 7. Normalized difference vegetation index (NDVI) for a 7136 ha portion of the Konza LTER. Brightness is proportional to NDVI. A) Original 33.0 m resolution; B) second renormalized image at 132 m cell width; C) continued renormalization to 264 m; D) 528 m resolution.

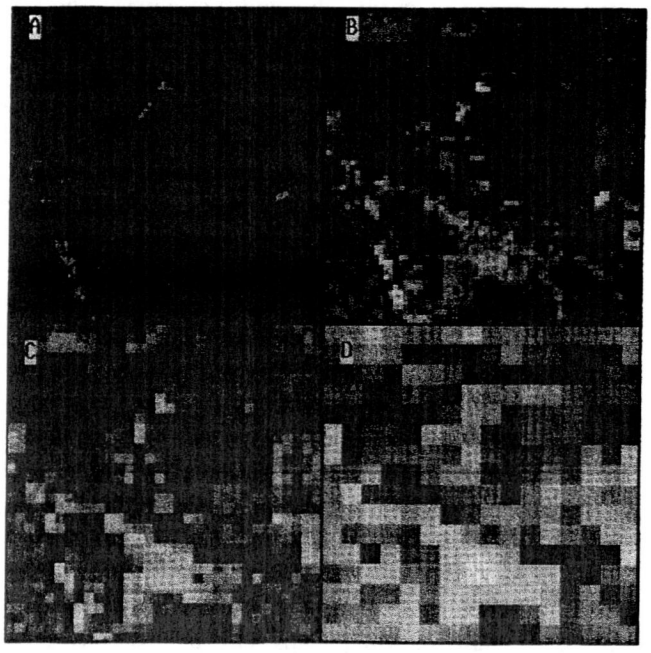

curve, both below and above $q=0$. Comparison of the Konza 132 m map (Fig. 7b) with those of the Sevilleta (Fig. 1) suggest that the riparian areas dominate the image at 132 m in the Konza, leading to similar $\tau(q)$ curves. At broad scales (300–2000 m), the semivariogram for Konza (Fig. 6 inset) exhibited a power law with an exponent equal to 0.105, corresponding to a fractal dimension of 1.94 (Burrough, 1981), which being close to 2, testifies to the homogeneous appearance of the NDVI at coarse resolution (Fig. 7d). Other processes, such as land use practices and experimental burning treatments that control patch boundaries visible at 66 m (Fig. 7a), were apparently more important at fine scales. Thus, multifractals illustrated a great potential to both: 1) classify landscapes that share similar $\tau(q)$ curves as being controlled by similar processes and 2) select scales at which to render landscape patterns controlled by particular processes.

Derivation of Semivariance by Renormalization

Our goal of aggregating fine scale maps of continuous and binary, or thematic, variables (Table 1) requires consideration of how changes in cell size relate to standard geostatistical properties. Here, we describe a fundamental relation between the geostatistics of continuous versus binary land cover variables. The relation has implications both for the expected values of geostatistical measurements and for the representation of ecologically relevant spatial features, such as stream networks and landforms.

Here we consider the indicator semivariance (Deutsch and Journel, 1992), defined as the semivariance of a binary indicator variable z_i at location i, which is assigned a value of 1 whenever a continuous variable y_i is greater than an arbitrary cutoff value and 0 otherwise; the transformation produces a binary map. After making the indicator transformation, the semivariance is computed from the z_i's as in Eq. (1). In the spirit of spatial renormalization (e.g., Gould and Tobochnik, 1988), it is useful to consider how the various configurations of zeros and ones within 2×2 blocks of cells contribute to the indicator semivariance and how these contributions change as a map is rendered at ever coarser resolution.

Recall again the majority renormalization rule (Turner, 1989), in which 2×2 cell blocks are inspected, and the entire block is relabeled according to whichever class is in the majority; ties are settled by flipping a coin. Thus, the proportion of a random, binary map that is still occupied after majority rule renormalization is $p'=3p^2(1-p)^2+4p^3(1-p)+p^4$. Terms in the equation describe the number of ways of obtaining two, three, or four occupied cells in a block such that the majority rule is satisfied. Iteration of the function reveals that maps beginning at $p=0.5$ remain so, while maps with $p<1/2$ converge on $p=0$; maps with $p>1/2$ converge on $p=1$. Thus, 1/2 is a nontrivial fixed point of the renormalization, reflecting the 50:50 rule by which ties are resolved during the spatial aggregation process. Iteration reveals a fundamental property of a map, in this case, whether a particular land cover class is in the majority, or not.

Here, we use renormalization to examine how the indicator semivariance behaves with a coarsening of scale. In so doing, we reveal fundamental spatial properties of the binary transformation $z_i \rightarrow \{0, 1\}$ of continuous variables and define characteristic densities and semivariances of random maps. The results provide a means of detecting spatial scales at which independence is achieved and makes standard geostatistical theory complementary to multifractal analyses.

For convenience, restricting the lag to $h=L=1$ (i.e., z_i is compared to z_{i+L} in the north, south, east, and west directions only) reveals that various block configurations produce particular sums of squared differences [Eq. (1)]. For example, in the trivial cases of empty or full blocks, all possible pairwise comparisons produce $(z_i-z_{i+L})^2=0$ because there is no within-block variance. However, with one or three occupied cells the respective sums of squared deviations equal 4. Two occupied cells situated orthogonally to one another produce a squared deviation of 4; diagonally arranged duplets yield a squared deviation of 8.

Thus, the configurations that contribute to nonzero values for the indicator semivariance are those with one, two, or three occupied cells. To maintain accurate intercell distances of $i+L$, we restrict the 2-cell cases to those having occupied neighbors in the cardinal directions, of which there are four configurations. Each relevant configuration occurs on a random map, or equivalently on a map rendered with cells of length equal to the range, at rates equal to $4p(1-p)^3$, $4p^2(1-p)^2$, and $4p^3(1-p)$ for the 1-, 2-, and 3-cell cases, respectively. Thus, upon renormalization, a map beginning with p occupied cells obtains a new proportion p' according to

$$p'=4p(1-p)^3+4p^2(1-p)^2+4p^3(1-p)$$
$$=4\sum_{m=1}^{3} p^m(1-p)^{4-m}. \quad (8)$$

The expected indicator semivariance for $h=L$ can be written using the renormalized probability. The number of blocks containing m occupied cells on a map is always $(E/L)^2 4p^m(1-p)^{4-m}$ since there are four equivalent rotations of each configuration. The expected semivariance is obtained by weighting the number of blocks of each configuration by the respective sum of squared deviations [Eq. (1); i.e., four in each case) and dividing by twice the number of comparisons, including those made in the empty and full blocks. Since there are eight cell-to-cell comparisons within each block, the total number of comparisons on the map is $8(E/L)^2$ and the semivariance.

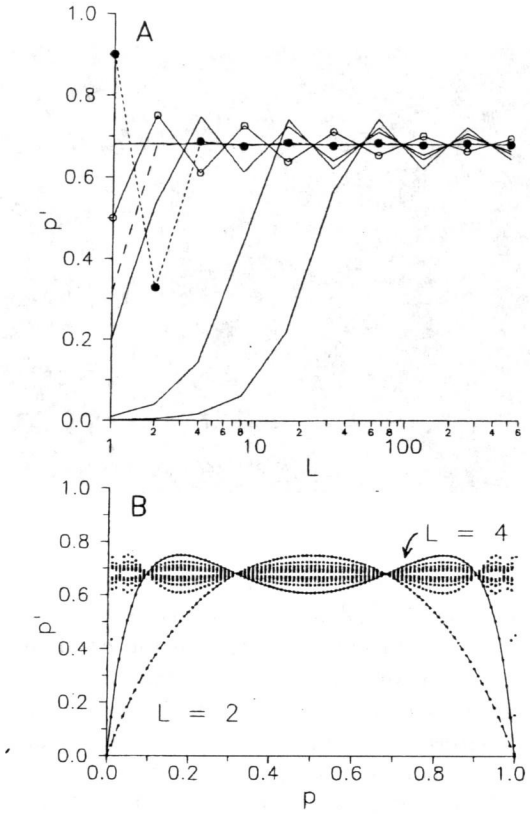

Figure 8. Simulated renormalization trajectories of the probability of having occupied cells at successively coarser scales [Eq. (8)]. A) Example trajectories as a function of the number of cells (L) along one edge of square renormalized random maps; B) successive probabilities p' obtained from initial probabilities p. The labeled curves indicate the renormalized values after changing to cell widths of 2 and 4 unit cells. As L increases, p' reaches a constant value of 0.68.

$$\gamma(h)=\frac{16(E/L)^2\sum p'^m(1-p')^{4-m}}{16(E/L)^2}$$

$$=\sum p'^m(1-p')^{4-m}. \qquad (9)$$

The effects of increases in block length, or equivalently lag, are investigated by iterating the renormalization relation, starting with a given p, to reveal the asymptotic behavior of the map upon aggregation. Transient behavior is common for one to 10 or more iterations, corresponding to increases in cell length L from 1 to 1024 or more (Fig. 8a). Eventually, all initial p values lodge at 0.68, which is a stable point of Eq. (8). Some initial p reach the stable point at finer scales than others, due to the nonlinear nature of the discrete mappings from one scale to the next (Fig. 8b). Some maps require >20 iterations to reach asymptotic behavior measurable to four decimal places. This is equivalent to increasing the original cell size L from 2^0 to 2^{20}, or decreasing the 10,000-m-wide LTER study sites to a width of 9.5 mm. In general, spatial aggregation of land cover maps will be governed by the transient dynamics with great sensitivity to the initial configuration of occupied cells.

To investigate the predicted indicator semivariance [Eq. (9)], we constructed binary maps by thresholding the Konza and Sevilleta maps at approximately $p=0.5$ (Fig. 9). We renormalized the maps by the indicator rule and measured the semivariance [Eq. (1)] at each scale. We predicted: 1) that the observed semivariance and p' would converge on $\gamma^*(h)$ and p^* as h approached the range, thereby indicating membership in the class of random maps, and 2) that the semivariance and density of images rendered at scales finer than the range would deviate from the fixed points, thereby indicating nonrandom structure. We included five random maps ($p=0.5$) of the same size for comparison with the empirical maps.

After the transient period, Eqs. (8) and (9) converge on a fixed point with coordinates $\gamma^*(h)$, p^* for all initial p (Fig. 10). Thus, the model predicts the well-known result that random maps exhibit the same semivariance at all scales. Renormalization of the empirical binary images (Fig. 9) produced trajectories of semivariances and associated probabilities that deviated from those of random maps (Fig. 10) until cell sizes approximated the range. We tested the ability of the model to predict $\gamma(L=32)$ and p^* of random maps. There was no significant difference between the renormalized probabilities and the predicted ($t=-1.67$, $P=0.17$, $N=5$) but the observed semivariances were significantly higher than expected ($t=8.77$, $P=0.0009$, $N=5$). Renormalizations based on small blocks are known to have small biases (Gould and Tobochnik, 1988) because of artifacts that creep in as two adjoining blocks conspire on the real map to produce configurations that are not represented in the model. Nonetheless, a better renormalization relation might be found that incorporates block-to-block correlations.

In light of sharing identical mass exponents at $L=4$ (i.e., cell widths of 114 m and 132 m in the Sevilleta and Konza, respectively; Fig. 6), the proximity of renormalized p and $\gamma(L)$ at these scales (Fig. 10) suggests the same similarity. However, since the Sevilleta trajectory explores a range of values, despite exhibiting identical mass exponents at all scales (Fig. 6), the semivariance and p alone appear insufficient to identify patterns driven by a given process.

There are rich implications for scale transformations of binary or thematic maps. First, the ultimate configuration of occupied cells at the coarse resolution is extremely dependent on, or sensitive to, the configuration of cells on the original map, since the number of iterations required to reach the stable probability varies with the original p (Fig. 8a). This is due to the way in which blocks of cells are first reclassified, only to form new blocks with their neighbors at a coarser resolution. Many permutations of occupied cells exist, leading to idiosyn-

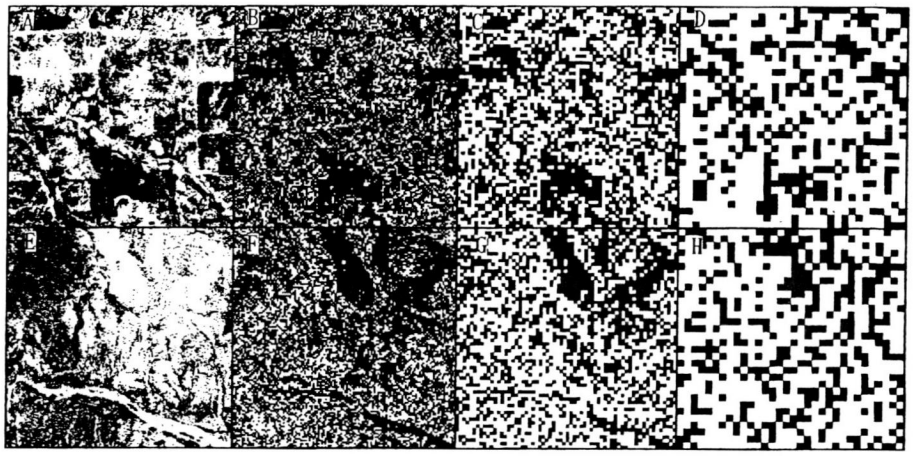

Figure 9. Renormalization of binary images for the Konza LTER (panels A–D) and the Sevilleta LTER (E–H). White regions indicate values below the 50th (Konza) and 66th (Sevilleta) percentiles of NDVI and LAI, respectively. The indicator rule was used in each case and the renormalized images magnified to show detail.

cratic neighborhood geometries or polygon shapes. Second, the origin of this sensitivity is implicit in the creation of the indicator variable. Specifically, once y_i is thresholded to 0 or 1, information is lost as to exactly how different the y values were in two adjacent cells. In some cases, adjacent cells may differ little, but if they span the classification threshold, they will be segregated into two classes, as would two neighboring cells with y values in opposite tails of the distribution. Thus, precision is sacrificed, and the price is uncertainty about the disparity between cells. Third, the indicator semivariance is extremely sensitive to measurement or classification errors on the original map, since errors both alter the initial p value and produce errors in the configurations. Fourth, the fluctuations in the probabilities with scale will induce fluctuations in the indicator semivariance.

In contrast, nonrandom binary maps have nontrivial spatial correlations among the block configurations (Milne, 1992) and a function other than Eq. (9) is needed for the expected semivariance. The spatial correlations among block configurations can be modeled by measuring the scale dependent, perhaps fractal, geometry of the configurations [Eq. (5)]. As above [Eq. (9)], all occupied cells that are in the orthogonal 2-cell configurations are retained while diagonally connected 2-cell blocks are ignored. Thus, assuming isotropy so that each of the four possible rotations of each block are included, the renormalization relation for the proportion p' becomes Eq. (10):

$$p'(L)=4/E^2\sum_{m=1}^{3} c_m L^{2-D(m)}, \qquad (10)$$

where $D(m)$ is the box dimension of blocks containing m occupied cells. The behavior of $p'(L)$ as a function of L will depend on the map. Analogous functions could be made if the number of occupied blocks varied logarithmically or exponentially with scale.

Figure 10. Renormalization trajectories of the semivariance and the probability of having occupied cells. Iteration of the model [Eqs. (8) and (9)] starting with various initial probabilities p yields the parabola which collapses to $\gamma^*(h)$ and p^* (dashed lines) at coarse scales. Analyses of empirical maps from the Sevilleta and Konza and of random maps (solid squares) are included. Numbers 114 and 132 indicate selected cell lengths (m) for the Sevilleta and Konza, respectively.

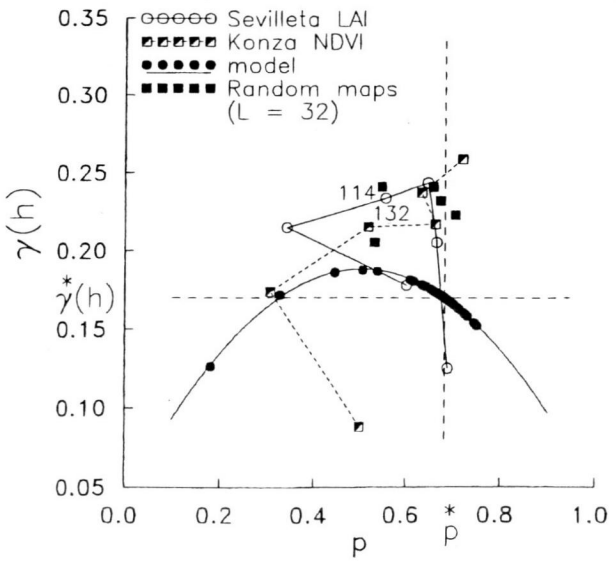

CONCLUSIONS

Our first goal was to identify major issues involving the use of MODIS as a source of ecological information. For one, new sensors involve an implicit change in scale from the traditional 1 m^2 quadrats used in the field to the 500–1000-m-wide cells. Changes in scale alter the apparent geostatistical properties of the landscape, including subpixel variation (i.e., the nugget), the apparent effect of processes that affect the nugget [Eq. (2)], the lags over which patterns are nonrandom, and the averaging accomplished by the coarse spatial resolution sensor. However, changes in scale provide an important tool with which ecologists can search for novel patterns of

system organization and dynamics. Simultaneously, relations are needed to translate patterns and estimates from one scale to another (King et al., 1991), as basic quantities such as the number of lakes on a landscape change with scale (Benson and MacKenzie, 1995). Second, knowledge of subcell patterning is needed to design and implement field campaigns to validate MODIS estimates. Clearly, geostatistical evaluations at subpixel scales are useful for identifying locations to sample mean values with least effort (Fig. 3). Third, ecologically relevant flow networks may be obscured by coarse resolution imagery obtained by averaging (Rodríguez-Iturbe and Rinaldo, 1998), as, for example, where detrital pools affect nutrient concentrations downstream, or where fires passing through networks of fuel effectively connect distant locations. Coarse depictions of landscapes may obscure ecologically relevant information that pertains to fine-scale processes.

Major errors may be produced if nonlinear functional relations are applied to linearly transformed imagery (Cale et al., 1983). Wilson (1979; 1983) explains that renormalization effectively drives a map into another region of parameter space. For that reason, we would expect the nonlinearly renormalized map to behave differently in a nonlinear model than a linearly rescaled map. Much as aeronautical engineers understand how to apply measurements made in wind tunnels to real aircraft, future ecological applications may be able to use multifractal scaling exponents (Fig. 6) to rescale coarse resolution predictions back to the ground. Reduced image resolution creates both tradeoffs and opportunities.

With daily estimates of fundamental biophysical variables, even at 1000 m resolution, the potential for driving fine-scale process models over relatively small study areas is profound and promises a robust, biophysical foundation upon which to build ecologies of populations, communities, landscapes, and ecosystems. In the same vein, coarse scale renderings of landscapes may challenge ecologists to identify limits to the spatial extents over which various processes operate, thereby leading to a clearer characterization of the relevant ecological hierarchies (Allen and Starr, 1982; O'Neill et al., 1986).

Our second major goal was to recommend strategies for spatially aggregating fine scale imagery. Tradeoffs here involve the dichotomy between continuous and thematic imagery. In general, coarse resolution land cover maps should be made from spatially averaged or renormalized continuous images to avoid errors created by aggregating fine-scale binary maps. Errors vary with the density of the binary images (Fig. 8) and scale (Fig. 6). After aggregating spectral bands separately in such a way as to preserve the multifractal structure (Fig. 6), we assume that classification methods that work for high resolution images will work for the aggregated images only if covariances are preserved. A related solution is to represent land cover at coarse scales with a vector that describes the relative percentages of land cover types observed at fine scale (Fig. 5).

Spatial aggregation of continuous variables creates opportunities for novel classifications. To filter variables at different scales, one could use spectral bands or derived variables that have been aggregated to different scales and resampled to a common scale before classification. For example, aggregation of near-infrared bands to very course scale to obtain independence of pixel values, combined with a finely resolved visible band, might enable better representation of advective energy fluxes due to high albedo from small features. Likewise, nonlinear mixing of spectral signatures at coarse resolution might be investigated by renormalizing each band to several scales and then using multivariate analysis to determine the band and scale combinations most related to the coarse resolution imagery. Recent work with "fractal regularizations" and multiscale data structures (Chou et al., 1994) provide examples. Thus, purposeful manipulation of image resolution through geostatistical analysis and spatial aggregation constitutes a general strategy for formulating new predictions based on remotely sensed imagery.

This research was funded in part by the Terrestrial Ecology Program, Office of Mission to Planet Earth, NASA (NAGW-4880), as part of the MODLERS project and by EPA 153-2244 subcontract to BTM. J. Briggs generously provided the Konza imagery. G. Shore, T. Maddux, K. Taugher, and E. Muldavin contributed substantially to construction of the Sevilleta LAI map. Suggestions from R. V. O'Neill and two anonymous reviewers broadened the context of the work. Sevilleta LTER Publication No. 141.

REFERENCES

Allen, T. F. H., and Starr, T. B. (1982), *Hierarchy: Perspectives for Ecological Complexity*, University of Chicago Press, Chicago, 310 pp.

Atkinson, P. M. (1997), On estimating measurement error in remotely sensed images with the variogram. *Int. J. Remote Sens.* 18:3075–3084.

Atkinson, P. M., and Curran, P. J. (1995), Defining an optimal size of support for remote sensing investigations. *IEEE Trans. Geosci. Remote Sens.* 33:768–776.

Barclay, H. (1998), Conversion of total leaf area to projected leaf area in lodgepole pine and Douglas-fir. *Tree Physiol.* 18:185–193.

Baret, F., and Guyot, G. (1991), Potentials and limits of vegetation indices for LAI and APAR assessment. *Remote Sens. Environ.* 35:161–173.

Barnes, W. L., Pagano, T. S., and Solomonson, V. V. (1998), Prelaunch characteristics of the Moderate Resolution Imaging Spectrometer (MODIS) on EOS-AM1. *IEEE Trans. Geosci. Remote Sens.* 36:1088–1100.

Benson, B. J., and MacKenzie, M. D. (1995), Effects of sensor spatial resolution on landscape structure parameters. *Landscape Ecol.* 10:113–120.

Bilonick, R. A. (1985), The space-time distribution of sulfate deposition in the northeastern United States. *Atmos. Environ.* 19:1829–1845.

Binney, J. J., Dowrick, N. J., Fisher, A. J., and Newman, M. E. J. (1993), *The Theory of Critical Phenomena: An Introduction to the Renormalization Group*, Oxford Science Publications, Oxford, 464 pp.

Box, E. O., Holben B. N., and Kalb, V. (1989), Accuracy of the AVHRR vegetation index as a predictor of biomass, primary productivity and net CO_2 flux. *Vegetatio* 80:71–89.

Burrough, P. A. (1981), Fractal dimensions of landscapes and other environmental data. *Nature* 294:241–243.

Burrough, P. A. (1983), Multiscale sources of spatial variance in soil. *J. Soil Sci.* 34:577–597.

Cale, W. G., O'Neill, R. V., and Gardner, R. H. (1983), Aggregation error in nonlinear ecological models. *J. Theor. Biol.* 100:539–550.

Chou, K. C., Willsky, A. S., and Benveniste, A. (1994), Multiscale recursive estimation, data fusion, and regularization. *IEEE Trans. Automat. Control* 39:464–478.

Churkina, G., and Running, S. W. (1998), Contrasting climatic controls on the estimated productivity of different biomes. *Ecosystems* 1:206–215.

Cohen, W. B., Spies, T. A., and Fiorella, M. (1995), Estimating the age and structure of forests in a multi-ownership landscape of western Oregon, U.S.A. *Int. J. Remote Sens.* 16:721–746.

Cooper, J. R., Gilliam, J. W., Daniels, R. B., and Robarge, W. P. (1987), Riparian areas as filters for agricultural sediment. *Soil Sci. Soc. Am. J.* 51:416–420.

Cressie, N. A. C. (1991), *Statistics for Spatial Data*,Wiley, New York, 900 pp.

Creswick, R. J., Farach, H. A., and Poole, C. P., Jr. (1992), *Introduction to Renormalization Group Methods in Physics*, Wiley, New York, 409 pp.

Crist, E., and Cicone, R. (1984), A physically-based transformation of Thematic Mapper data—the TM Tasseled Cap. *IEEE Trans. Geosci. Remote Sens.* GE-22: 256–263.

Deutsch, C. V., and Journel, A. G. (1992), *GSLIB: Geostatistical Software Library and User's Guide*, Oxford University Press, Oxford, 340 pp.

Dubayah, R. C. (1994), Modeling a solar radiation topoclimatology for the Rio Grande River Basin. *J. Veg. Sci.* 5: 627–640.

Feder, J. (1988), *Fractals*, Plenum, New York, 283 pp.

Forman, T. T. (1995), *Land Mosaics*, Cambridge University Press, Cambridge, 632 pp.

Franklin, J. F., Bledsoe, C. S., and Callahan, J. T. (1990), Contributions of the Long-Term Ecological Research Program. *BioScience* 40:509–523.

Friedl, M. A., Davis, F. W., Michaelsen, J., and Moritz. M. A. (1995), Scaling and uncertainty in the relationship between the NDVI and land-surface biophysical variables: an analysis using a scene simulation-model and data from FIFE. *Remote Sens. Environ.* 54:233–246.

Gould, H., and Tobochnik, J. (1988), *An Introduction to Computer Simulation Methods: Applications to Physical Systems. Part 2*, Addison-Wesley, Reading, MA, pp. 320–695.

Halsey, T. C., Jensen, M. H., Kadanoff, L. P., Procaccia, I., and Shraiman, B. I. (1986), Fractal measures and their singularities: the characterization of strange sets. *Phys. Rev. A* 33:1141–1151.

Hill, M. O. (1973), The intensity of spatial pattern in plant communities. *J. Ecol.* 61:225–236.

Hurlbert, S. H. (1984), Pseudoreplication and the design of ecological field experiments. *Ecol. Monogr.* 54:187–211.

Jelinski, D. E., and Wu, J. (1995), The modifiable areal unit problem and implications for landscape ecology. *Landscape Ecol.* 11:129–140.

Jensen, M. H., Kadanoff, L. P., Libchaber, A., Procaccia, I., and Stavans, J. (1985), Global universality at the onset of chaos: results of a forced Rayleigh–Bénard experiment. *Phys. Rev. Lett.* 55:2798–2801.

Jensen, M. E., Burman, R. D., and Allen, R. G. (1989), *Evapotranspiration and Irrigation Water Requirements*, American Society of Civil Engineers, New York, 332 pp.

Johnson, A. R., Milne, B. T., and Wiens, J. A. (1992), Diffusion in fractal landscapes: simulations and experimental studies of Tenebrionid beetle movements. *Ecology* 73:1968–1983.

Jupp, D. L. B., Strahler, A. H., and Woodcock, C. E. (1988a), Autocorrelation and regularization in digital images I: Basic theory. *IEEE Trans. Geosci. Remote Sens.* 26:463–473.

Jupp, D. L. B., Strahler, A. H., and Woodcock, C. E. (1988b), Autocorrelation and regularization in digital images II: Simple image models. *IEEE Trans. Geosci. Remote Sens.* 27: 247–258.

Justice, C., Hall, D., Salomonson, V., et al. (1998), The Moderate Resolution Imaging Spectroradiometer (MODIS): land remote sensing for global change research. *IEEE Trans. Geosci. Remote Sens.* 36:1228–1249.

Keitt, T. H., Urban, D. L., and Milne, B. T. (1997), Detecting critical scales in fragmented landscapes. *Conserv. Ecol.* 1(1):4 [http://www.consecol.org/vol1/iss1/art4].

King, A. W., Johnson, A. R., and O'Neill, R. V. (1991), Transmutation and functional representation of heterogeneous landscapes. *Landscape Ecol.* 5:239–253.

Levin, S. A. (1992), The problem of pattern and scale in ecology. *Ecology* 73:1943–1967.

Loreto, V., Pietronero, L., Vespignani, A., and Zapperi, S. (1995), Renormalization group approach to the critical behavior of the forest-fire model. *Phys. Rev. Lett.* 75:465–468.

Mandelbrot, B. B. (1982), *The Fractal Geometry of Nature*, Freeman, New York, 468 pp.

Mandelbrot, B. B., and Wallis, J. R. (1969), Some long-run properties of geophysical records. *Water Resour. Res.* 5: 967–988.

Menenti, M., Ritchie, J. C., Humes, K. S., et al. (1996), Estimation of aerodynamic roughness at various spatial scales. In *Scaling Up in Hydrology Using Remote Sensing* (J. B. Stewart, E. T. Engman, R. A. Feddes, and Y. Kerr, Eds.), Wiley, New York, pp. 39–58.

Milne, B. T. (1988), Measuring the fractal geometry of landscapes. *Appl. Math. Comput.* 27:67–79.

Milne, B. T. (1991), Lessons from applying fractal models to landscape patterns. In *Quantitative Methods in Landscape Ecology* (M. G. Turner and R. H. Gardner, Eds.), Springer-Verlag, New York, pp. 199–235.

Milne, B. T. (1992), Spatial aggregation and neutral models in fractal landscapes. *Am. Naturalist* 139:32–57.

Milne, B. T. (1998), Motivation and benefits of complex systems approaches in ecology. *Ecosystems* 1:449–456.

Milne, B. T., and Johnson, A. R. (1993), Renormalization relations for scale transformation in ecology. In *Some Mathematical Questions in Biology: Predicting Spatial Effects in Ecological Systems* (R. H. Gardner, Ed.), American Mathematical Society, Providence, RI, pp. 109–128.

Milne, B. T., Johnson, A. R., Keitt, T. H., Hatfield, C. A., David, J., and Hraber, P. (1996), Detection of critical densities associated with piñon-juniper woodland ecotones. *Ecology* 77:805–821.

Milne, B. T., Johnson, A. R., and Matyk, S. (1999), ClaraT: Instructional software for fractal pattern generation and analysis. In *Landscape Ecological Analysis: Issues and Applications* (J. M. Klopatek and R. H. Gardner, Eds.), Springer-Verlag, New York, pp. 304–332.

O'Neill, R. V., and Rust, B. (1979), Aggregation error in ecological models. *Ecol. Model.* 7:91–105.

O'Neill, R. V., DeAngelis, D. L., Waide, J. B., and Allen, T. F. H. (1986), *A Hierarchical Concept of Ecosystems*, Princeton University Press, Princeton, NJ, 253 pp.

O'Neill, R. V., Gardner, R. H., Milne, B. T., Turner, B. T., and Jackson, B. (1991), Heterogeneity and spatial hierarchies. In *Ecological Heterogeneity* (J. Kolasa and S. T. A. Pickett, Eds.), Springer-Verlag, New York, pp. 85–96.

O'Neill, R. V., Hunsaker, C. T., Timmins, S. P., et al. (1996), Scale problems in reporting landscape pattern at the regional scale. *Landscape Ecol.* 11:169–180.

Openshaw, S. (1984), *The Modifiable Areal Unit Problem*, CATMOG 38, GeoBooks, Norwich, UK.

Pachepsky, Y. A., Ritchie, J. C., and Gimenez, D. (1997), Fractal modeling of airborne laser altimetry data. *Remote Sens. Environ.* 61:150–161.

Parsons, W. F. J., Knight, D. H., and Miller, S. L. (1994), Root gap dynamics in lodgepole pine forest: nitrogen transformations in gaps of different size. *Ecol. Appl.* 4:354–362.

Pierce, L. L., and Running, S. W. (1995), The effects of aggregating sub-grid land surface variation on large-scale estimates of net primary productivity. *Landscape Ecol.* 10: 239–253.

Prince, S. D., and Goward, S. N. (1995), Global primary production: a remote sensing approach. *J. Biogeogr.* 22: 815–835.

Rich, P. M., Hughes, G. S., and Barnes, F. J. (1993), Using GIS to reconstruct canopy architecture and model ecological processes in pinyon–juniper woodlands. In *Proceedings of the Thirteenth Annual ESRI User Conference*, Vol. 2, pp. 435–445.

Rodríguez-Iturbe, I., and Rinaldo, A. (1998), *Fractal River Basins: Chance and Self-Organization*, Cambridge University Press, Cambridge, 547 pp.

Schlesinger, W. H. (1991), *Biogeochemistry: An Analysis of Global Change*, Academic, San Diego, 443 pp.

Solé, R. V., and Manrubia, S. C. (1995), Are rain-forests self-organized in a critical state? *J. Theor. Biol.* 173:31–40.

Sommerer, J. C., and Ott, E. (1993), Particles floating on a moving fluid: a dynamically comprehensible physical fractal. *Science* 259:335–339.

Stanley, H. E., Amaral, L. A. N., Buldyrev, S. V, et al. (1996), Scaling and universality in animate and inanimate systems. *Physica A* 231:20–48.

Stauffer, D., and Stanley, H. E. (1989), *From Newton to Mandelbrot: A Primer in Theoretical Physics*, Springer-Verlag, New York.

Stoms, D. M., Bueno, M. J., and Davis, F. W. (1997), Viewing geometry of AVHRR image composites derived using multiple criteria. *Photogramm. Eng. Remote Sens.* 63:681–689.

Strauss, D. (1992), The many faces of logistic-regression. *Am. Stat.* 46:321–327.

Turner, M.G. (1989), Landscape ecology: the effect of pattern on process. *Annu. Rev. Ecol. Syst.* 20:171–197.

Turner, D. P., Cohen, W. B., Kennedy, R. E., Fassnacht, K. S., and Briggs, J. M. (1999), Relationships between leaf area index and Landsat TM spectral vegetation indices across three temperate zone sites. *Remote Sens. Environ.* 70:52–68.

Ustin, S. L., Wessman, C. A., Curtiss, B., Kasischke, E., Way, J., and Vanderbilt, V. C. (1991), Opportunities for Using the EOS Imaging Spectrometers and Synthetic Aperture Radar in Ecological Models. *Ecology* 72:1934–1945

White, J. D., and Running, S. W. (1994), Testing scale dependent assumptions in regional ecosystem simulations. *J. Veg. Sci.* 5:687–702.

Wilson, K. G. (1979), Problems in physics with many scales of length. *Sci. Am.* 241:158–179.

Wilson, K. G. (1983), The renormalization-group and critical phenomena. *Rev. Mod. Phys.* 55:583–600.